SCIENTIFIC REPORTS

OPEN

SUBJECT AREAS:
NANOSTRUCTURES
DRUG DELIVERY
TRANSLATIONAL RESEARCH
MEDICAL TOXICOLOGY

Received
12 July 2012

Accepted
29 October 2012

Published
13 November 2012

Correspondence and requests for materials should be addressed to G.J.N. (niegj@nanoctr.cn) or Y.L.Z. (zhaoyuliang@ihep.ac.cn)

* These authors contributed equally.

Effects of gestational age and surface modification on materno-fetal transfer of nanoparticles in murine pregnancy

Hui Yang[1]*, Cuiji Sun[1]*, Zhenlin Fan[1,6], Xin Tian[1], Liang Yan[2], Libo Du[3], Yang Liu[3], Chunying Chen[1], Xing-jie Liang[1], Gregory J. Anderson[4], Jeffrey A. Keelan[5], Yuliang Zhao[1,2] & Guangjun Nie[1]

[1]CAS Key Laboratory for Biomedical Effects of Nanomaterials & Nanosafety, National Center for Nanoscience and Technology, Beijing, 100190 China, [2]Institute of High Energy Physics, Chinese Academy of Sciences, Beijing, 100049 China, [3]Institute of Chemistry, Chinese Academy of Sciences, Beijing, 100190 China, [4]Iron Metabolism Laboratory, Queensland Institute of Medical Research, Royal Brisbane Hospital, Brisbane, Queensland, 4029 Australia, [5]School of Women's and Infant's Health, University of Western Australia, King Edward Memorial Hospital, Subiaco, Perth, WA, Australia, [6]College of Pharmaceutical Sciences, Jilin University, Changchun, 130021, China.

Nanoparticle exposure in pregnancy may result in placental damage and fetotoxicity; however, the factors that determine fetal nanoparticle exposure are unclear. Here we have assessed the effect of gestational age and nanoparticle composition on fetal accumulation of maternally-administered nanomaterials in mice. We determined the placental and fetal uptake of 13 nm gold nanoparticles with different surface modifications (ferritin, PEG and citrate) following intravenous administration at E5.5-15.5. We showed that prior to E11.5, all tested nanoparticles could be visualized and detected in fetal tissues in significant amounts; however, fetal gold levels declined dramatically post-E11.5. In contrast, Au-nanoparticle accumulation in the extraembryonic tissues (EET) increased 6–15 fold with gestational age. Fetal and EET accumulation of ferritin- and PEG-modified nanoparticles was considerably greater than citrate-capped nanoparticles. No signs of toxicity were observed. Fetal exposure to nanoparticles in murine pregnancy is, therefore, influenced by both stage of embryonic/placental maturation and nanoparticle surface composition.

With the accelerating development and use of nanomaterials in cosmetic, medical and pharmaceutical applications[1–3], the importance of assessing the biodistribution characteristics and potential risks of nanomaterials to human health is growing[4,5]. As the risk of exposure to nanomaterials in pregnancy increases[6–8], so does the opportunity for exposure to the developing fetus - one of the most vulnerable subgroups of society[9,10]. Accordingly, the materno-fetal transfer of nano-scale substances has become of great interest in assessing the safety of nanomaterials in pregnancy for medical purposes[11,12] and the associated risk of growth and developmental defects in the fetus[13,14]. There have only been a limited number of studies in this area. In rodents, titanium oxide (TiO_2) nanoparticles administered early in pregnancy have been showed to reach the fetal brain and cause various developmental abnormalities[15]. These results supported earlier findings using C60 fullerene nanoparticles[16]. A more recent study found that ~35 or ~70 nm nanoparticles composed of TiO_2 or silica, administered in late pregnancy at high concentrations, were able to cross the murine placenta and enter fetal tissues[17]; fetal toxicity and growth restriction secondary to effects on placenta growth, structure and function were observed. In contrast, surface-modified silica nanoparticles were relatively non-toxic[17]. Wick et al., using an *ex vivo* human placental perfusion model, showed that fluorescent polystyrene particles with a diameter of up to 240 nm were taken up by the placenta and were able to cross the placenta without affecting the viability of the placental tissue[7]. This study suggests that the placental barrier in late pregnancy provides only partial fetal protection against nano-sized materials.

These reports collectively show considerable uncertainty regarding the mechanism, extent and consequence of materno-fetal transfer of nanoparticles. While there is good evidence that maternal exposure to various toxic nanomaterials in high doses can have adverse effects on fetal growth and development[17,18], few studies have directly assessed feto-placental uptake and transfer, and the assumption that toxicity is mediated by direct fetal tissue exposure to nanomaterials has not been generally proven. It is unclear how nanoparticles accumulate in placenta and other intrauterine tissues and the extent to which nanoparticles accumulate in (and cross) the placenta and enter fetal tissues.

The placenta is composed primarily of specialised blastocyst-derived trophoblast cells which constitute the "placenta barrier"[19–21], the permeability of which determines the selective transfer of substance between maternal and fetal circulations. This occurs mainly via a range of mechanisms that include passive diffusion, facilitated diffusion, active transport, endocytosis, paracellular entry and water-filled transplacental channels[9,10,22,23]. The specific transplacental transport mechanisms for nanomaterials have not been elucidated, although it is known that the surface properties of nanomaterials significantly influence their biological properties[24,25].

Placental structure, cellular composition, function and blood flow change with gestational age[26,27], which alters placental uptake and transport. Placental development begins at embryonic day 3.5 (E3.5) in mice and by E8.5 the formation of villi and the elaboration of the placental blood supply has commenced. Establishment of hemotrophic nutrition leads to direct exchange of substances between the fetal and maternal blood circulations[28]. Evidence shows that this stage, beginning at around E10 in mice, corresponds to the last two trimesters of gestation in humans[29]. Despite some anatomical and structural differences between the murine and human placenta, the functional "barrier" for both species is relatively similar, depending primarily on either one (human) or three (murine) layers of blastocyst-derived trophoblast cells[29,30]. The monohemochorial structure of the human placenta renders it more permeable than the murine placenta, while the murine yolk sac also plays a considerable role in endocytotic substance transfer, particularly in early gestation prior to the establishment of the placental circulation[30]. Fetuses exhibit distinct differences in susceptibility to xenobiotics throughout development according to the stage of organogenesis and metabolic maturation[31,32]. Therefore, it is critical to take into account both the stage of feto-placental development and physicochemical properties of nanomaterials when evaluating nanoparticle transplacental transport and fetotoxicity during pregnancy.

In this study, we investigated the biodistribution and fetotoxicity of gold (Au) nanoparticles throughout murine pregnancy. We employed three types of surface modification to explore the effects of nanomaterial functionality on materno-placental-fetal biodistribution: coating with an endogenous protein (ferritin) for optimal biocompatibility, coating with PEG for optimal pharmacokinetics and reduced opsonization, and coating with a stablizing anionic material (citrate) to explore the effects of negative charge on placental and fetal biodistribution. Our studies help to clarify some of the factors that govern materno-fetal transfer of nanoparticles in mice, and provide important biosafety information relating to nanomaterials and their biomedical applications in pregnancy.

Results

Materno-fetal transfer of Au-nanoparticles. Three Au-nanoparticles ~13 nm were synthesized: A) a ferritin nanocage enclosing a pair of Au nanoclusters inside (Au-Ft), B) Au-nanoparticles capped with polyethylene glycol-5000 (Au13-PEG) and C) Au-nanoparticles coated with sodium citrate (Au13-CT) (Fig. 1a,b). These nanomaterials are suitable for investigation of materno-fetal transfer as they have good biocompatibility, low toxicity *in vivo* and quantitative measurement in tissues[33]. Furthermore, these nanoparticles are too large to cross the placenta by paracellular diffusion, but small enough to be able to be accommodated by so-called transtrophoblastic channels or pinocytotic/transcytotic processes[23]. Cryo-electron microscopy (Cryo-EM) and transmission electron microscopy (TEM) images showed that all three nanoparticle formulations were monodispersed with average size of ~13 nm (Fig. 1c). The zeta potential of Au-Ft, Au13-PEG and Au13-CT, which indicates the degree of repulsion between adjacent charged nanoparticles, was −1.6, −6.0 and −17.0 mV, respectively (Fig. 1d). Nanoparticle suspensions or PBS were injected into the tail vein of pregnant mice at embryonic E5.5 to E15.5 in 184 μg/ml injection solution (Fig. 1e).

The Au content in the heart, liver, spleen, lung, kidney, extraembryonic tissues (EET: placenta, umbilical cord, amnion and uterine wall) and fetus was measured by inductively-coupled plasma mass-spectrometry (ICP-MS) 5 h after injection (Figs. 2 and 3 and Supplementary Table 1 and 2). There were no consistent differences in Au accumulation in the maternal organs with pregnancy or gestational age, although between the three different nanoparticles the levels of accumulation of Au in the organs, such as liver, spleen and kidney varied significantly (Supplementary Table 1 and 2). The absolute concentrations of Au in fetus and EET after administration with different nanoparticles across gestation are shown in Fig. 2a–c. All nanoparticles accumulated in EET throughout gestation; there were notable differences depending on nanoparticle surface composition and gestational age (black bars, Fig. 2a–c). Importantly, in early gestation (up to E9.5), Au levels in the fetus following Au-Ft and Au13-PEG nanoparticle administration were relatively high (>1000 ng/g) and comparable to levels in the EET, whereas from E11.5 onwards fetal Au levels were markedly diminished (white bars, Fig 2a,b). Fetal Au13-CT levels were about 50–120 ng/g prior to E9.5 and were negligible from E11.5 onwards (Fig. 2c). The dramatic change in fetal accumulation at E11.5 was due to a precipitous decline in maternal-fetal transport, as seen by the reduction in fetal:EET Au ratios at different gestational ages (Fig. 2d).

To determine the kinetics of fetal Au-nanoparticle biodistribution, the rate of Au-nanoparticle accumulation in the fetus and the EET was measured after a single maternal injection of Au-Ft, Au13-PEG or Au13-CT at 0.9 μg Au/g body weight. At E8.5 administration, the Au concentrations in the fetal tissues and EET remained relatively high for at least 72 h after injection, although the Au13-PEG nanoparticles took considerably longer (24 h) to reach maximal levels than the other two (2 h) (Fig. 2e–g). With Au13-CT nanoparticles a marked and steady decline in both EET and fetal levels was seen from 2 h post administration (Fig. 2g). As shown in Fig. 2h, the total Au content in fetal tissues (adjusted for fetal weight) reached maximal levels after 5 h and remained relatively constant for at least 72 h in the Au-Ft groups, whereas accumulation of the Au13-PEG nanoparticles plateaued after 24 h, in agreement with the Au concentration data (Fig. 2e,f). On the other hand, the Au13-CT nanoparticles reached only low levels 2 h after injection and were then steadily cleared from the EET and fetus during the experiment (Fig. 2g). At E11.5, administration of Au-Ft resulted in extremely low Au levels in fetal tissues (0.02% of total Au dose; Supplementary Table 2) and similar Au levels in the EET as seen in that at E8.5 group (Fig. 2i *vs.* e).

Au-nanoparticle biodistribution in pregnant mice. It is widely recognized that, in addition to size, surface modification is of critical importance in determining the biodistribution of nanoparticles via their interactions with macromolecules, pinocytotic pathways and cellular transport machinery[33]. We employed Au-Ft, Au13-PEG and Au13-CT nanoparticles as examples of biological, PEGylated and anionic nanomaterials to investigate their biodistribution and accumulation following maternal intravenous injection during pregnancy. In the Au-Ft group, Au was observed largely in maternal liver and kidney 5 h after injection (Supplementary Table 1 and 2), similar to the biodistribution reported in non-pregnant mice[34]. Interestingly, ferritin-encaged Au also significantly accumulated in the EET with increasing gestational age and placental size (Supplementary Table 2), but less accumulated in lung and heart (Fig. 2 and Supplementary Table 2). In the Au13-CT group, considerably more Au was distributed in liver and spleen, with relatively lower levels of Au detected in other organs, including EET and fetus. The combined effects of gestational age and nanoparticle functionalization are illustrated in Fig. 3, in which Au accumulation as a percentage of total Au dose is compared in liver, EET and fetus at two time points (E7.5 and 11.5) before and after the period of critical change in fetal delivery. The mid-pregnancy increase in EET accumulation and

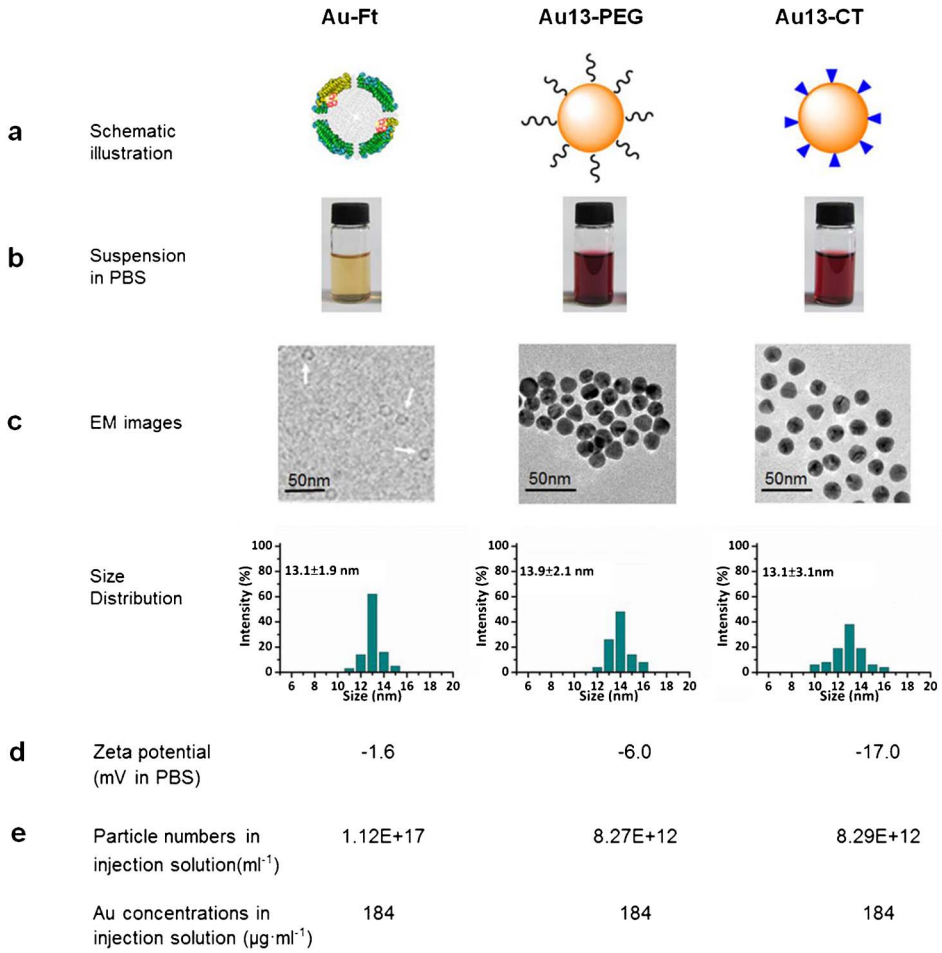

Figure 1 | Characterization of Au-Ft, Au13-PEG and Au13-CT nanoparticles. (a) Schematic illustration of the synthesized Au-nanoparticles (Au-Ft, Au13-PEG and Au13-CT); (b) Images of suspended Au-nanoparticles in PBS; (c) Cryo-electron microscopy (Cryo-EM) image and size distribution of Au-Ft, and TEM images of Au13-PEG and Au13-CT and their corresponding size distributions; (d) Zeta potential of Au-Ft, Au13-PEG and Au13-CT in PBS; (e) Particle numbers and Au concentrations of the three nanoparticles used in these studies.

decrease in fetal accumulation is clearly evident, as is the lack of uptake of Au13-Ct nanoparticles by the fetus and preferential accumulation in the maternal liver (Fig. 3c). A small but significant decline in liver Au accumulation was also observed in this group. For the Au13-Ft and –PEG nanoparticles, fetal accumulation of Au declined from around 0.6–0.8% of the total dose at E7.5 to 0.02–0.06% at E11.5 (Fig. 3a, b). These findings are consistent with a previous report[35], in which Au-nanoparticles administered late in pregnancy had almost no materno-fetal transfer. PEG surface modification dramatically decreased Au-nanoparticle organ accumulation in liver and spleen and facilitated a more even distribution among all the organs and tissues, including EET and fetus (before E11.5). The amounts of Au in the EET and the fetus were comparable prior to E11.5, whereas in later stages of pregnancy the amounts in the EET were much greater, in accordance with the increase in placental size (Supplementary Table 1 and 2). It is worth noting that the recovery of total dose in the biodistribution studies was only about 35%, 15%, and 50% for the Au-Ft, Au13-PEG, and Au13-CT nanoparticles, respectively. The remaining Au is likely to be distributed in bloodstream, muscle and other organs not collected. It is also likely that a portion of Au injected will be excreted via the kidneys or the GI tract, depending on the Au preparation. These results showed that the biodistribution of Au-nanoparticles in pregnant mice differs according to their coating and surface properties.

During gestation, changes in the properties of the placenta and/or reticuloendothelial system (RES) might alter the extent of infiltration of exogenous nanoparticles into the fetus and the EET[36], consequently altering the biodistribution of nanoparticles in pregnant mice. Gestational age had little impact on Au accumulation in non-reproductive organs (Supplementary Table 1). In contrast, the Au concentrations in the EET of pregnant mice were consistently higher than levels in the uteri of non-pregnant mice (Fig. 2a–c and Supplementary Table 1 and 2). These results suggest that the accumulation of exogenous nanoparticles in the uterine area (including uterine wall, yolk sac, umbilical cord, amnion and placenta) is increased with pregnancy, particularly late in gestation when placental blood flow and mass is maximal. Taken together, these data indicate that nanoparticle composition and surface properties determine their biodistribution and EET/placental accumulation in a gestational age-dependent fashion.

Visualisation and tissue distribution of Au-nanoparticles. Tissue distribution of elemental Au was examined using hard X-ray microfocus beamline synchrotron imaging of uterine sections from E8.5 mice, fixed 5 h after Au-Ft treatment. The Au content in the uterus increased significantly following Au-Ft administration compared with control tissues treated with vehicle (Fig. 4a *vs.* c). The Au signal was concentrated in the fetal tissue close to the implantation site (red arrows in Fig. 4a, c, e) as well as the uterine wall. These images are consistent with the arrival of Au-Ft nanoparticles via the maternal circulation, penetrating the placenta tissue located around implantation site, and eventually entering the fetus. As a

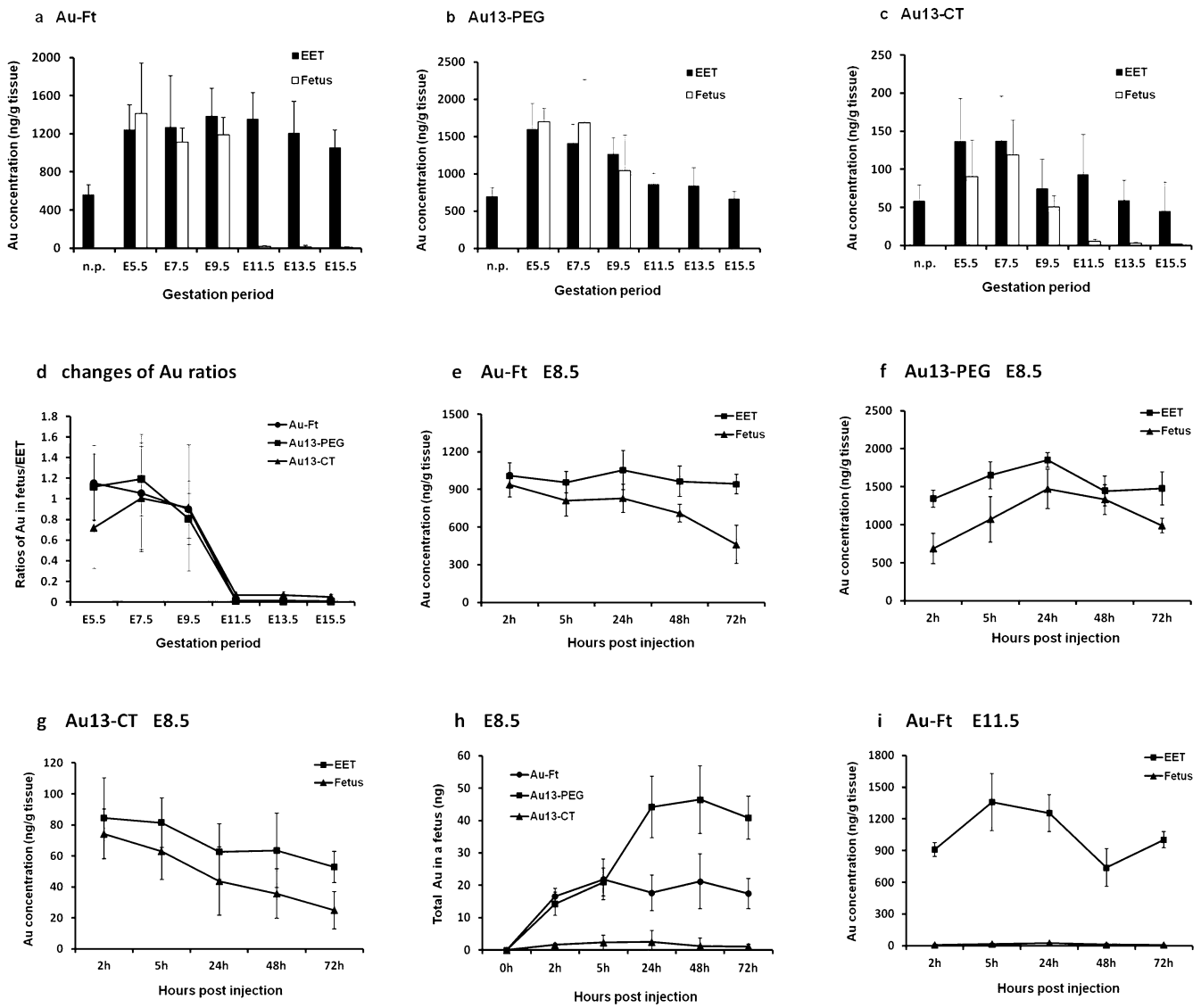

Figure 2 | Au accumulation in fetuses and extraembyronic tissues (EET) after a single dose of Au-nanoparticle preparation at different stages of gestation. Au-Ft (a), Au13-PEG (b) and Au13-CT (c) were administered from E5.5 to E15.5. Au content was evaluated by ICP-MS 5 h after Au administration. (d) The ratios of Au in fetus/EET after administration of different nanoparticles at different gestation stages. The dynamic changes in Au concentration in fetuses and EET are shown for (e) Au-Ft, (f) Au13-PEG, and (g) Au13-CT. (h) Total Au content in fetuses after one administration of Au-nanoparticles to pregnant mice at E8.5. The dynamic changes in Au concentrations in fetuses and EET after Au-Ft injection at E11.5 are shown in (i). Each data set represents the mean ± s.d. (n=6).

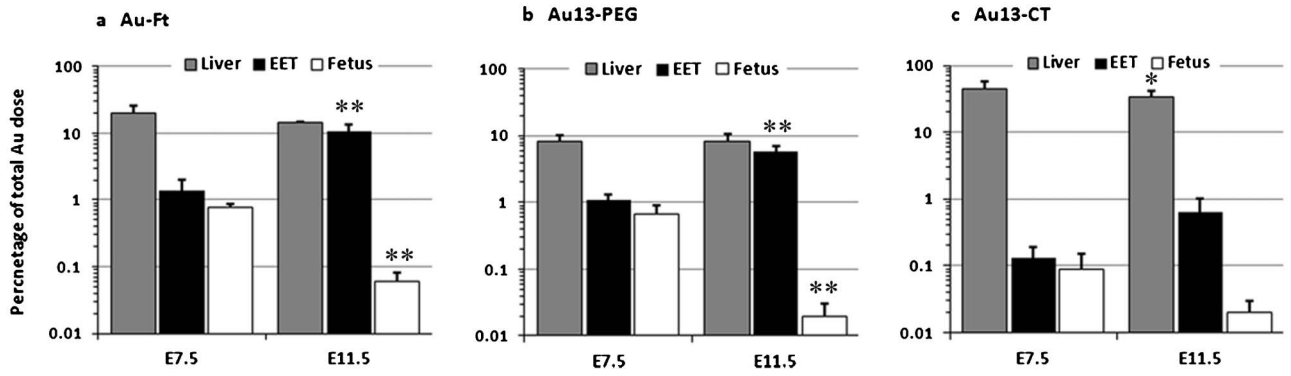

Figure 3 | Au accumulation as a percentage of total recovered dose in maternal liver, extraembyronic tissues (EET) and fetuses after Au-nanoparticle preparation at E7.5 and E11.5. Au-Ft (a), Au13-PEG (b) and Au13-CT (c) were administered at E7.5 and 11.5. Au content (mean ± s.d.) was evaluated by ICP-MS 5 h after Au administration. *, $P<0.5$; ** $P<0.001$, E11.5 *vs.* E7.5 (ANOVA, n=6).

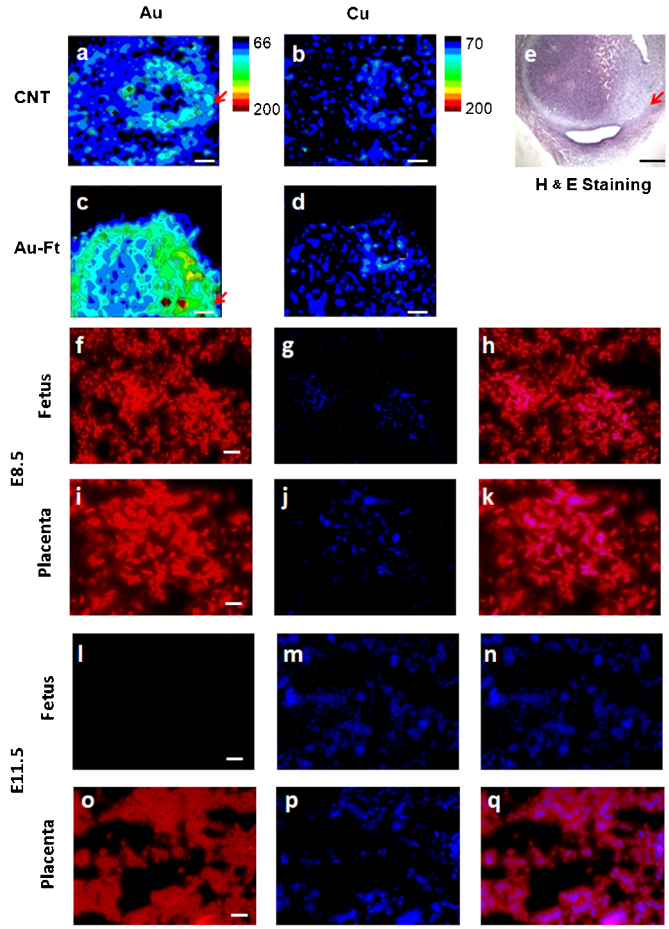

Figure 4 | Biodistribution of Au-nanoparticles in fetal and EET. Fetal Au accumulation was seen by X-ray microprobe synchrotron imaging near the implantation site (red arrows) and uterine wall (c), while Cu (as negative control) showed low and uniformed distribution in the entire fetus (b and d), at E8.5. Scale bar is 1 mm. Hematoxylin eosin (H&E) staining (e) of a corresponding section shows the uterine shape and orientation. CNT refers to the control group. Intrinsic Au fluorescence was observed in the fetal and placental tissue sections at E8.5 (f-k) and E11.5 (l-q). No apparent Au-Ft fluorescence was observed in the fetal tissue at E11.5. Shown are red Au-Ft fluorescence (f, i, l, o), blue Hoechst 33342 labeled nuclei (g, j, m, p), and merged images (h, k, n, q). The scale bar is 8 μm.

control, the signal from Cu was detected faintly in uterine sections with or without Au-Ft exposure with a non-specific distribution pattern (Fig. 4b, d). To investigate the microscopic distribution of Au-Ft in feto-placental tissues, we observed far red fluorescence of Au nanoclusters after Au-Ft administration (Fig. 4f–q). Specific fluorescent signals for Au-Ft were largely localized in the fetal at E8.5 (Fig. 4f, h) and placental tissues at both E8.5 (Fig. 4i, k) and E11.5 (Fig. 4o, q), but not in the fetus at E11.5 (Fig. 4l, n); this may indicate that the Au taken up by the placenta and the fetus represents intact Au nanocluster structures within the ferritin shell.

To further demonstrate the tissue distribution of Au-nanoparticles, we examined the Au13-PEG and Au13-CT nanoparticles in the fetus and the placental tissues by TEM 5 h after administration at different gestational stages. At E8.5, both Au13-PEG and Au13-CT nanoparticles were found in the fetus (Fig. 5a, e) as well as the placenta (Fig. 5b, f); however, at E11.5, nanoparticles could only be found in the placenta (Fig. 5d, h), but not in the fetus (Fig. 5c, g). These results suggest that Au13-PEG and Au13-CT existed as intact nanoparticles in the fetus and the placenta and confirmed that their biodistribution varied according to stage of embryonic/placental maturation.

To observe live imaging of Au-Ft nanoparticles in uterine tissues, Au-Ft nanoparticles were administered by tail vein injection to pregnant mice at E8.5 at a final Au dose of 7.2 μg/g body weight. Ventral fluorescent signals were recorded with a Maestro™ *in vivo* optical imaging system. About 5 h after injection, a "V-shape" catenular structure (consistent with the uterus) was observed in the underbelly of pregnant mice as indicated by the white dotted line in Fig. 6d, while no fluorescent signals were obtained from the control mouse (Fig. 6b). An intense fluorescent signal was also observed in liver (indicated by white arrow, Fig. 6d) in the central abdomen. These fluorescent signals could be visualised for up to 7 h. To further confirm the *in vivo* imaging results, the ventral skin, muscle and intestines were removed and the organs inside pelvic cavity and chest were exposed and visualized. Distinct fluorescence signals in uterus and liver (marked by arrows in Fig. 6h) were observed and those signals coincided with the signals obtained in the *in vivo* images (Fig. 6d). No fluorescent signal was obtained from other organs, such as heart and lung. In controls, no fluorescence was observed in untreated mice (Fig. 6f).

Effects on fetal and postnatal growth and fertility. Au-nanoparticles show low or no toxic effects both *in vitro* and *in vivo*[33]. Au-Ft with natural protein as the shell of the nanocage is believed to possess good biocompatibility[37] and similar protein-based nanomedicine platforms have widely been used for drug delivery[38]. We administered Au-Ft, Au13-PEG and Au13-CT to pregnant mice at early (E5.5) and late (E13.5) gestation, and monitored the dams and their offspring during pregnancy, delivery and 8 weeks postnatally. Throughout the entire experimental period, none of the pregnant mice exhibited symptoms of abnormality or stress. All the pups in the nanoparticle-treated groups delivered at term and the fetal numbers were comparable to controls. Pup viability and body weight were not significantly different among control and experimental groups (Table 1 and Supplementary Fig. 1). Histological examinations of the pups also confirmed that there were no detectable tissue damage in any of the sections obtained from the kidney and liver in the three Au-nanoparticle treated pups compared to the control pups (Supplementary Fig. 2). Postnatal growth of offspring and development of eyes and ears was similar between all groups. All offspring had the same mating ability 6–8 weeks after birth (Table 1).

These findings suggest that not only does fetal exposure vary according to gestational age and placental maturation, but fetal exposure does not necessarily equate with developmental toxicity, as there were no signs of developmental abnormalities or weight reductions in any of the offspring studied from the Au-nanoparticles-treated groups ($\sim 8.3\times10^{12}$ Au-nanoparticles/ml for Au13-PEG or Au13-CT and $\sim 1.1\times10^{17}$ Au-nanoparticles/ml for Au-Ft in injection solution). Au-nanoparticles are known to be biologically benign, unlike other some other materials tested such as silica, TiO_2 and Cd[17,39]. Chu et al. described the administration of ~3 nm mercaptopropionic acid-coated CdTe/CdS quantum dots to pregnant mice later in pregnancy at E15.5[39], and reported very low amounts of Cd were detected in the fetus, between 20–100 ng/g body weight. This is similar to the late gestation fetal Au concentrations we observed in our study, but far less than the Au levels in fetus exposed in early gestation. In pregnant rats, uptake of 1.4 nm and 18 nm gold nanoparticles ($\sim 3\times10^{13}$ in injection solution) into secondary target organs has been shown to be size dependent after intravenous application[40]. While no comparable data exists on nanoparticle exposure of the fetus in human pregnancy, *ex vivo* perfusion studies conducted on term placentas suggest that PEGylated Au-nanoparticles <30 nm ($\sim 1.6\times10^{10}$–1.6×10^{11} Au-nanoparticles/ml in perfusion solution) readily accumulate in the placenta but do not cross to the fetal circulation, at least within a short time-frame[41].

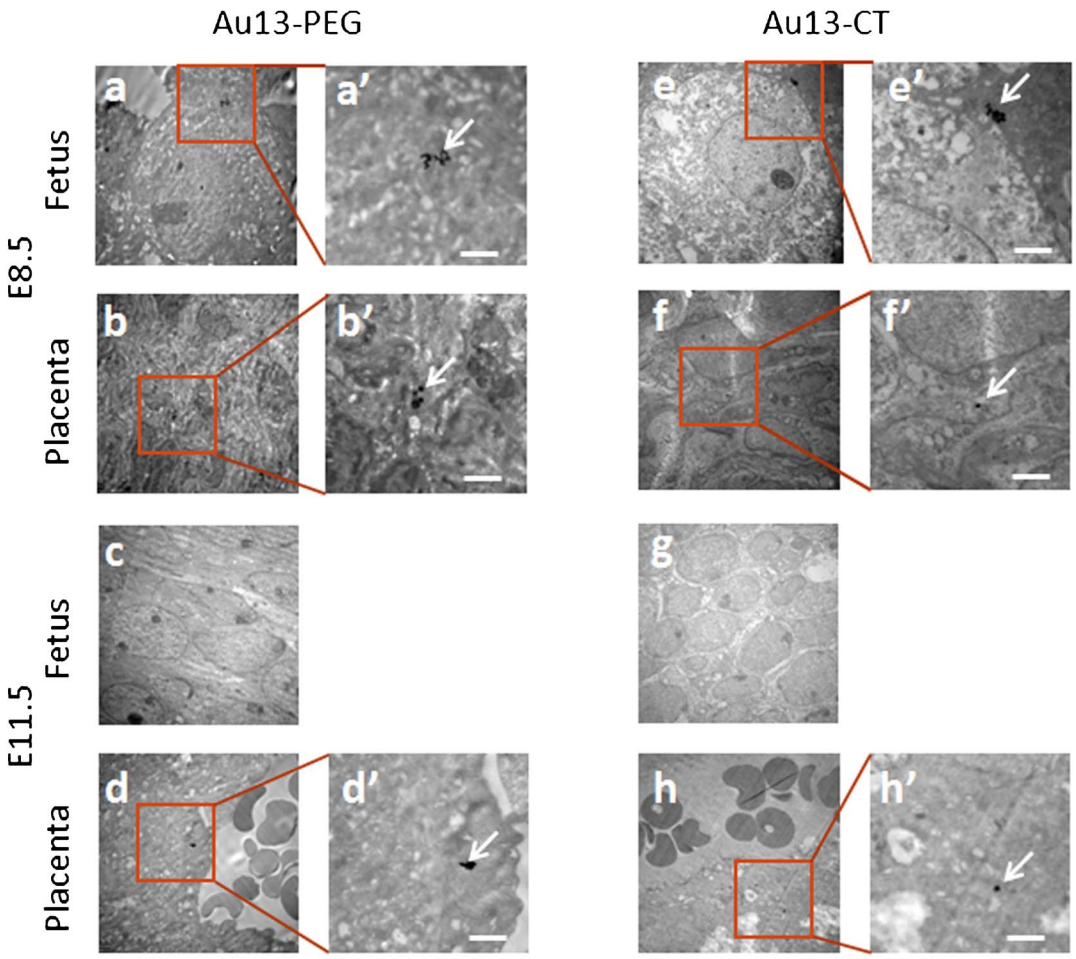

Figure 5 | TEM images of placenta and fetal tissues after Au-nanoparticle administration. Au13-PEG or Au13-CT nanoparticles were intravenously injected into pregnant mice at E8.5 and E11.5. Au-nanoparticles were present in the fetus (a, e) and the placenta (b, f) of E8.5 mice, as well as the placenta (d, h) of E11.5 mice, but not in the fetus at E11.5 (c, g); amplified images are shown in the inserts. The scale bar is 1 μm.

Discussion

Understanding the factors that determine the embryonic distribution and transplacental passage of nanoparticles is of growing importance as the likelihood of exposure to nanomaterials in pregnancy increases. Early gestation is a particularly important period as the mother may not be aware of her pregnancy and chances of unintended exposure are higher. In addition, less mature embryos are potentially more susceptible to nanoparticle toxicity. In this study we have made the important observation that a critical time window exists in murine pregnancy which determines the extent of fetal exposure to maternally-administered gold nanomaterials. After this time window, which is between E9.5 and E11.5 and coincides with maturation of the murine placental blood supply and barrier function of the placenta at around E10, there is a dramatic reduction in fetal exposure to maternally-delivered gold nanoparticles. Our findings also indicate that the surface composition of gold nanoparticles determines their rate and extent of passage and the degree of fetal exposure in a gestational age-dependent fashion. Surface functionality affected feto-placental transfer and accumulation as would be predicted from its known effects on maternal pharmacokinetics and interactions with endocytotic transport processes. Particles with a negative surface coating are known to exhibit reduced cellular-uptake characteristics[42], consistent with the extremely low levels of anionic Au13-CT particles observed in the EET and fetus. In contrast, the particles with improved biocompatibility/bioavailability (PEG and ferritin-coated) had similar levels of feto-placental accumulation, with PEG coating conferring an increased rate of transfer consistent with its ability to reduce clearance rates. The size of nanoparticles is another important parameter which may influence placental/fetal penetration and biodistribution of nanoparticles and we have not investigated the effects of size in the current study. Thus, the present study has addressed important issues relating to some of the factors governing placental uptake, passage and fetal exposure. This information is needed to pave the way for effective and safe biomedical applications of nanoparticles in pregnancy. Our novel findings in murine pregnancy have significant biomedical and biosafety implications for nanoparticle administration in pregnancy in humans. Further work is required to assess the importance of species differences and define the cellular mechanisms underlying the variable permeability of nanoparticles across the placental barrier.

Methods

Synthesis and characterization of Au-nanoparticles. Ferritin Au nanostructures (Au-Ft) were synthesized by the "points of control" method as previously reported[34], in which the ferroxidase active sites of apoferritin were used as bioreactors to synthesize Au clusters inside a ferritin nanocage. Cryo-electron microscopy (Cryo-EM) of Au-Ft was performed in an FEI Titan Krios cryo-electron microscope (Fig. 1a). Citrate-coated Au-nanoparticles (Au13-CT) with 13 nm mean diameters were synthesized as previously reported[43], and PEGylated 13 nm Au-nanoparticle (Au13-PEG) were prepared by reacting citrate-coated Au-nanoparticles with a 2500-fold excess of thiolated PEG-5000 for 3 h at 25°C[44]. The morphology and size of Au13-CT and Au13-PEG were evaluated using transmission electron microscopy (TEM, JEM-200CX, Jeol Ltd., Japan). The nanoparticles' surface charge (zeta potential, mV) and size distribution were determined using a ZetaSizer Nano series Nano-ZS (Malvern Instruments Ltd., Malvern, UK). The suspensions were sonicated for 5 min before use.

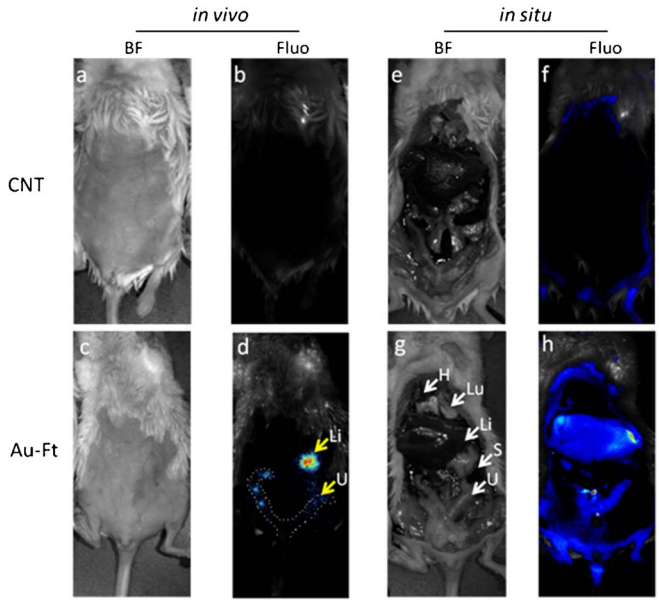

Figure 6 | *In vivo* fluorescence images of pregnant mice following Au-Ft administration at E8.5. Au-Ft was administered to pregnant mice at 7.2 μg/g body weight and the images show the fluorescence signal from embryonic tissue 5 h after injection. *In vivo* bright field (BF) and fluorescence (Fluo) images of control mouse without Au-Ft treatment (a, b); Au-Ft treated mouse (c, d). After *in vivo* imaging, the mice were sacrificed and the ventral skin, muscle and intestines were removed to expose the organs for *in situ* imaging (e–h). *In situ* BF and Fluo images of Au-Ft treated mouse (g, h); control mouse without Au-Ft treatment (e, f). H, heart; Lu, lung; Li, liver; S, spleen; U, uterus. The images are representative of four mice administered with Au-Ft.

Animals. CD-1 mice (20–25 g) were obtained from Beijing Vital River Laboratories, Beijing, China. All animal experiments were approved by the Animal Ethics Committee of the Medical School, Beijing University. After acclimation for 1 week, the mice were mated and the presence of a vaginal plug was confirmed 12–14 h later, designated as embryonic day 0.5 (E0.5). Pregnant mice were given injections via tail vein of 100–200 μl nanoparticles (0.9–7.2 μg Au/g body weight) diluted in phosphate buffered saline solution (PBS) at different gestation age between E5.5 and E15.5. Each experimental group consisted of n=6 animals unless otherwise indicated.

ICP-MS. The tissue Au-nanoparticle concentrations were assessed by quantitative inductively coupled plasma mass spectrometry (ICP-MS) measurement. Five h after Au-Ft, Au13-PEG or Au13-CT injection (100–200 μl, 0.9 μg Au/g body weight), mice were anaesthetized, euthanized and the tissues, including heart, liver, spleen, lung and kidney were excised and weighed. Uteri were opened, fetuses were excised and remaining tissues were designated extraembryonic tissues (EET, Supplementary Fig. 3). Excised tissues were digested in *aqua fortis* (nitric acid: hydrochloric acid 3:1). After adjusting the solution volume to 2 ml using 2% nitric acid and 1% hydrochloride acid (1:1), gold assays were performed using an ELAN DRC e ICP-MS instrument (Perkin Elmer, Massachusetts, USA).

TEM analysis of tissue sections. Pregnant mice at E8.5 and E11.5 were treated with 100–200 μl Au13-PEG or Au13-CT (0.9 μg Au/g body weight). The mice were anaesthetized 5 h after injection. The placenta and fetus were excised and fixed in 2.5% glutaraldehyde for 2 h. Small pieces of tissues collected from these samples were washed with PBS, postfixed in sodium cacodylate buffered 1.5% osmium tetroxide for 60 min at 4°C, dehydrated using a series of ethanol concentrations, and embedded in Epon resin. The samples were examined under a Hitachi H-7650 transmission electron microscope (Hitachi, Tokyo, Japan).

Tissue localization of Au-Ft by fluorescent microscopy. Pregnant mice of E8.5 and E11.5 were injected with 7.2 μg Au/g body weight of Au-Ft. 5 h later, the fetus and placenta were excised, processed and cryo-sectioned on a Leica CM3050S cryostat (Leica Microsystems, Wetzlar, Germany). Nuclei were stained with Hoechst 33342. Au nanocluster fluorescent signals were examined via an inverted fluorescence microscope (MD2500-3HF-FL, Leica Microsystems, Wetzlar, Germany) equipped with a Nuance™ multispectral imaging system (CRi, Woburn, MA, USA). To obtain the Au-Ft signal, the ex/em filters were set at 535 ± 25 nm and 590 LP, respectively; for Hoechst 33342 signal, the ex/em filters were set at 350 ± 25 nm and 420 LP, respectively.

X-ray microbeam synchrotron imaging. Pregnant mice of E8.5 were injected with 100–200 μl Au-Ft (7.2 μg Au/g body weight) or PBS vehicle. The pregnant mice were sacrificed and the uteri and fetuses were fixed in 4% formaldehyde solution (pH 7.4) for 24 h, followed by dehydration and embedding in paraffin. Sections of 5 μm were cut and mounted onto Kapton film, supported by a clear acrylic frame. The specimens were analyzed by X-ray fluorescence mapping using hard X-ray microfocus beamline (BL15U) at Shanghai Synchrotron Radiation Facility (electron energy 12 keV, pixel size 100 nm and the acquisition time 3s per pixel).

***In vivo* and *in situ* imaging.** Five h after Au-Ft (7.2 μg Au/g body weight) injection, *in vivo* fluorescent images of live mice were obtained using a Maestro™ *in vivo* spectrum imaging system (CRi, Woburn, MA, USA) at excitation: emission 576–621:635 nm. After *in vivo* imaging, the mice were sacrificed and the ventral skin, muscle and intestines were removed. Organs inside pelvic cavity, abdominal cavity and chest were exposed for *in situ* fluorescent imaging on the same spectrum imaging system.

Pregnancy outcome, offspring growth, development and fertility. Nanoparticle (7.2 μg Au/g body weight) injections (or saline controls) were carried out once a day on two consecutive days in early gestation (E5.5 and E6.5) and late gestation (E13.5 and E14.5), respectively. After nanoparticle administration, pregnant mice were observed and checked at least three times a day after E18.5 and the time of delivery recorded. Dams were allowed to deliver spontaneously and nurse their pups until 5 weeks post partum. Total litter size and the numbers of live and dead pups were recorded on postnatal day 0 (PND0), PND4 and postnatal week 5 (PNW5). Body weight and tail length were recorded until 5 weeks after delivery. To examine offspring fertility, at 8 weeks after birth one male and three female offspring from the same treatment group were housed in the same cage for 10 days or until a vaginal plug was confirmed.

Histopathological examination of the major organs of the newborn mice. On postnatal day 1 (PND1) of the three gold nanoparticles treated and untreated dams, their pups were picked and putted on ice to faint, then dissected to get the various organs, including liver and kidney. The tissues were fixed with 10% formalin for 48 h, embedded in paraffin blocks, and then sliced into 5 μm in thickness on Leica CM1850 microtome. The bright-field images of hematoxylin-eosin (H&E) staining sections were acquired with a Leica DM1-3000B microscope equipped with a Nikon DXM1200 color CCD camera (Nikon Instruments Inc., Melville, NY).

Table 1 | Pregnant mice reproductive outcomes and offspring growth and development

	Gestation index (%)*	No. of live pups/pregnant female	Viability index PND4 (%)†	Average weight of pups on birth (g)	pups open eyes (post natal day)	Viability index PNW5 (%)‡	Offspring copulation index (%)§
Control	100	15	100	1.8	14	100	100
Au-Ft-E5.5	100	15	96.3	1.6	15	96.3	100
Au-Ft-E13.5	100	12	100	1.7	14	100	100
Au13-CT-E5.5	100	13	96.8	1.7	14	96.8	100
Au13-CT-E13.5	100	14	100	1.8	15	92.9	100
Au13-PEG-E5.5	100	14	100	1.8	14	100	100
Au13-PEG-E13.5	100	14	100	1.6	15	100	100

*Gestation index = (No. of females that delivered live pups/No. of pregnant females) × 100. †Viability index on PND 4 (%) = (No. of live pups on postnatal day 4/No. of live pups on postnatal day 0)×100. ‡Viability index PNW5 (%)= (No. of live pups on postnatal week 5/No. of live pups on postnatal day 0)×100. §Offspring mice copulation index (%) = (No. of offspring female mice with successful copulation/No. of offspring female mice paired)×100; Control mice were injected the same amount of PBS. No statistically significant changes were observed between groups or over time throughout the duration of the study.

Statistical analysis. All results are presented as means ± standard deviation (s.d.). Statistical significance in the differences between different groups was evaluated by LSD t-tests or Tukey's method after analysis of variance (ANOVA).

1. Bowman, D. M., van Calster, G. & Friedrichs, S. Nanomaterials and regulation of cosmetics. *Nature Nanotech.* **5**, 92 (2010).
2. Petros, R. A. & DeSimone, J. M. Strategies in the design of nanoparticles for therapeutic applications. *Nature Rev. Drug Discov.* **9**, 615–627 (2010).
3. Augustin, M. A. & Sanguansri, P. Nanostructured materials in the food industry. *Adv. Food Nutr. Res.* **58**, 183–213 (2009).
4. Maynard, A. D. *et al.* Safe handling of nanotechnology. *Nature* **444**, 267–269 (2006).
5. Oberdorster, G., Oberdorster, E. & Oberdorster, J. Nanotoxicology: an emerging discipline evolving from studies of ultrafine particles. *Environ. Health Perspect.* **113**, 823–839 (2005).
6. Saunders, M. Transplacental transport of nanomaterials. *Wiley Interdiscip. Rev. Nanomed. Nanobiotech.* **1**, 671–684 (2009).
7. Wick, P. *et al.* Barrier capacity of human placenta for nanosized materials. *Environ. Health Perspect.* **118**, 432–436 (2010).
8. Keelan, J. A. Nanotoxicology: nanoparticles versus the placenta. *Nature Nanotech.* **6**, 263–264 (2011).
9. Myllynen, P., Pasanen, M. & Vahakangas, K. The fate and effects of xenobiotics in human placenta. *Expert. Opin. Drug Metab. Toxicol.* **3**, 331–346 (2007).
10. Syme, M. R., Paxton, J. W. & Keelan, J. A. Drug transfer and metabolism by the human placenta. *Clin. Pharmacokinet.* **43**, 487–514 (2004).
11. Alexis, F., Pridgen, E., Molnar, L. K. & Farokhzad, O. C. Factors affecting the clearance and biodistribution of polymeric nanoparticles. *Mol. Pharm.* **5**, 505–515 (2008).
12. Peer, D. *et al.* Nanocarriers as an emerging platform for cancer therapy. *Nature Nanotech.* **2**, 751–760 (2007).
13. Ema, M., Kobayashi, N., Naya, M., Hanai, S. & Nakanishi, J. Reproductive and developmental toxicity studies of manufactured nanomaterials. *Reprod. Toxicol.* **30**, 343–352 (2010).
14. Bar-Ilan, O., Albrecht, R. M., Fako, V. E. & Furgeson, D. Y. Toxicity assessments of multisized gold and silver nanoparticles in zebrafish embryos. *Small* **5**, 1897–1910 (2009).
15. Takeda, K. *et al.* Nanoparticles transferred from pregnant mice to their offspring can damage the genital and cranial nerve systems. *J. Health Sci.* **55**, 95–102 (2009).
16. Tsuchiya, T., Oguri, I., Yamakoshi, Y. N. & Miyata, N. Novel harmful effects of [60]fullerene on mouse embryos in vitro and in vivo. *FEBS Lett.* **393**, 139–145 (1996).
17. Yamashita, K. *et al.* Silica and titanium dioxide nanoparticles cause pregnancy complications in mice. *Nature Nanotech.* **6**, 321–328 (2011).
18. Shimizu, M. *et al.* Maternal exposure to nanoparticulate titanium dioxide during the prenatal period alters gene expression related to brain development in the mouse. *Part. Fibre. Toxicol.* **6**, 20 (2009).
19. Burton, G. J., Jauniaux, E. & Charnock-Jones, D. S. Human early placental development: potential roles of the endometrial glands. *Placenta* **28 Suppl A**, S64–69 (2007).
20. Chae, J. I. *et al.* Proteomic analysis of the extraembryonic tissue from cloned porcine embryos. *Mol. Cell. Proteomics* **5**, 1559–1566 (2006).
21. Jansson, T. & Powell, T. L. Role of the placenta in fetal programming: underlying mechanisms and potential interventional approaches. *Clin. Sci. (Lond)* **113**, 1–13 (2007).
22. Schneider, H. & Miller, R. K. Receptor-mediated uptake and transport of macromolecules in the human placenta. *Int. J. Dev. Biol.* **54**, 367–375 (2010).
23. Menezes, V., Malek, A. & Keelan, J. A. Nanoparticulate drug delivery in pregnancy: placental passage and fetal exposure. *Curr. Pharm. Biotech.* **12**, 731–742 (2011).
24. Jia, G. *et al.* Cytotoxicity of carbon nanomaterials: single–wall nanotube, multi-wall nanotube, and fullerene. *Environ. Sci. Technol.* **39**, 1378–1383 (2005).
25. Li, Y. Y. *et al.* Chirality of glutathione surface coating affects the cytotoxicity of quantum dots. *Angew. Chem. Int. Ed.* **50**, 5860–5864 (2011).
26. Krantz, K. E., Panos, T. C. & Evans, J. Physiology of maternalfetal relationship through the extracorporeal circulation of the human placenta. *Am. J. Obstet. Gynecol.* **83**, 1214–1228 (1962).
27. Schneider, H. The role of the placenta in nutrition of the human fetus. *Am. J. Obstet. Gynecol.* **164**, 967–973 (1991).
28. Watson, E. D. & Cross, J. C. Development of structures and transport functions in the mouse placenta. *Physiology* **20**, 180–193 (2005).
29. Georgiades, P., Ferguson-Smith, A. C. & Burton, G. J. Comparative developmental anatomy of the murine and human definitive placentae. *Placenta* **23**, 3–19 (2002).
30. Enders, A. C. & Blankenship, T. N. Comparative placental structure. *Adv. Drug Deliver. Rev.* **38**, 3–15 (1999).
31. Luebke, R. W. *et al.* The comparative immunotoxicity of five selected compounds following developmental or adult exposure. *J. Toxicol. Environ. Health B Crit. Rev.* **9**, 1–26 (2006).
32. Miller, M. S. Transplacental lung carcinogenesis: molecular mechanisms and pathogenesis. *Toxicol. Appl. Pharmacol.* **198**, 95–110 (2004).
33. Khlebtsov, N. & Dykman, L. Biodistribution and toxicity of engineered gold nanoparticles: a review of in vitro and in vivo studies. *Chem. Soc. Rev.* **40**, 1647–1671 (2011).
34. Sun, C. *et al.* Controlling assembly of paired gold clusters within apoferritin nanoreactor for in vivo kidney targeting and biomedical imaging. *J. Am. Chem. Soc.* **133**, 8617–8624 (2011).
35. Sadauskas, E. *et al.* Kupffer cells are central in the removal of nanoparticles from the organism. *Part. Fibre. Toxicol.* **4**, 10 (2007).
36. Nicklin, S. & Billington, W. D. Macrophage activity in mouse pregnancy. *J. Reprod. Immunol.* **1**, 117–126 (1979).
37. Wang, W., Knovich, M. A., Coffman, L. G., Torti, F. M. & Torti, S. V. Serum ferritin: Past, present and future. *Biochim. Biophys. Acta* **1800**, 760–769 (2010).
38. Maham, A., Tang, Z., Wu, H., Wang, J. & Lin, Y. Protein-based nanomedicine platforms for drug delivery. *Small* **5**, 1706–1721 (2009).
39. Chu, M. *et al.* Transfer of quantum dots from pregnant mice to pups across the placental barrier. *Small* **6**, 670–678 (2010).
40. Semmler-Behnke, M. *et al.* Biodistribution of 1.4-and 18-nm gold particles in rats. *Small* **4**, 2108–2111 (2008).
41. Myllynen, P. K. *et al.* Kinetics of gold nanoparticles in the human placenta. *Reprod. Toxicol.* **26**, 130–137 (2008).
42. Qiu, Y. *et al.* Surface chemistry and aspect ratio mediated cellular uptake of Au nanorods. *Biomaterials* **31**, 7606–7619 (2010).
43. Frens, G. Controlled nucleation for the regulation of the particle size in monodisperse gold suspensions. *Nature* **241**, 20–22(1973).
44. Cho, W. S. *et al.* Acute toxicity and pharmacokinetics of 13 nm-sized PEG-coated gold nanoparticles. *Toxicol. Appl. Pharmacol.* **236**, 16–24 (2009).

Acknowledgments

This work was supported by National Basic Research Program of China (973 Program 2012CB934000, 2011CB933400) and NSFC (10979011; 30900278; 31000452). G.N. gratefully acknowledges the support of Chinese Academy of Sciences Hundred Talents Program. JK and GA are grateful recipients of Visiting Professorships from the Chinese Academy of Sciences.

Author contributions

H.Y., Y.Z. and G.N. designed the study, analysed the data and wrote the manuscript. C.S., Z.F., X.T., L.Y. and L.D. performed experiments. C.C., Y.L. and X.L. contributed to discussions and analytical tools. G.A. and J.K. analysed the data and wrote the manuscript. G.N. supervised the project. All Authors discussed the results and commented on the manuscript.

Additional information

Supplementary Information accompanies this paper at http://www.nature.com/scientificreports

Competing financial interests: The authors declare no competing financial interests.

How to cite this article: Yang, H. *et al.* Effects of gestational age and surface modification on materno-fetal transfer of nanoparticles in murine pregnancy. *Sci. Rep.* **2**, 847; DOI:10.1038/srep00847 (2012).